Supporting Information

Low loading of CoRe/TiO_2 for efficient hydrodeoxygenation of levulinic acid to γ-valerolactone

Zuojun Wei [a,b], Qing Li [a,b], Yuran Cheng [a,b], Mei Dong [c], Zuyi Zhang [a,b], Xinmiao Zhu [a,b], Yingxin Liu [c],* and Yong Sun[d],*

[a] Key Laboratory of Biomass Chemical Engineering of the Ministry of Education, College of Chemical and Biological Engineering, Zhejiang University, 38 Zheda Road, Xihu District, Hangzhou 310027, P.R. China.

[b] Institute of Zhejiang University-Quzhou, 78 Jiuhua Boulevard North, Quzhou 324000, P.R. China

[c] College of Pharmaceutical Science, Zhejiang University of Technology, 18 Chaowang Road, Xiacheng District, Hangzhou 310014, P.R. China

[d] College of Energy, Xiamen University, Xiamen 361102, P.R. China

*** Corresponding author:**

Professor Yingxin Liu, E-mail address: yxliu@zjut.edu.cn, phone: 0571-88320064;

Professor Yong Sun, E-mail address: E-mail: sunyong@xmu.edu.cn

Total numbers of pages: 13

Total numbers of Tables: 3

Total numbers of Figure: 3

Table of contents

Catalyst characterization S2
Products analysis S3
Table S1 ..... S5
Table S2 ..... S7
Table S3 ..... S8
Figure S1. ..... S9
Figure S2. ..... S10
Figure S3. ..... S11
References S12

Catalyst characterization

X-ray powder diffraction (XRD) patterns were recorded with an XRD-600 diffractometer (Shimadzu Co., Japan) using a Cu Kα radiation (λ = 0.15406 nm) in a Bragg-Brentano parafocusing optics configuration (40 kV, 40 mA). Samples were scanned from 10 ° to 80 ° with a scanning rate of 4 °·min^{-1} and a step size of 0.02 °. The crystalline phases were identified by reference to the JCPDS database.

BET specific surface areas and pore structures were measured by pulsed nitrogen adsorption-desorption method at -196 °C using an ASAP 2010 instrument (Micromeritics Instrument Co.). Prior to N_2 physisorption, the samples were degassed under vacuum at 250 °C overnight. The specific surface area was calculated by using the Brunauer-Emmett-Teller (BET) method, and the pore size distribution and pore volume were measured by Barrett-Joyner-Halenda (BJH) analysis from the adsorption branch of the isotherms.

High resolution transmission electron microscopy (HRTEM) images were obtained using a Tecnai G2 F30 S-Twin instrument (FEI Co., USA) operated at an accelerating voltage of 300 kV. Samples were prepared by dispersing the catalyst

powder in ethanol under ultrasound for 15-20 min and then dropping the suspension onto a copper grid coated with carbon film. Particle size distribution of metal nanoparticles in the sample was determined from the corresponding STEM image by measuring the sizes of more than 100 particles.

X-ray photoelectron spectroscopy (XPS) spectra were obtained using an Escalab Mark II X-ray spectrometer (VG Co., United Kingdom) equipped with a magnesium anode (Mg Kα = 1253.6 eV), 50 eV pass energy, a 0.2 eV kinetic energy step and 0.1 s dwelling time. Energy corrections were performed using a 1s peak of the pollutant carbon at 284.6 eV. The sample was prepared by pressing the catalyst powder onto the surface with silver sol gel.

Products analysis

The products were analyzed with an Agilent 7890 GC equipped with an HP-5 capillary column (30.0 m × 0.32 mm × 0.25 μm) and a flame ionization detector. The injector temperature was set at 250 °C and the sampling volume was 0.4 μl. The detector temperature was 260 °C. The split ratio was 1:10. The column temperature was raised from 70 °C to 230 °C at a heating rate of 5 °C·min^{-1} and then maintained at 230 °C for 5 min. GVL and LA were quantified by using n-dodecane as an internal standard. GC-MS analysis was performed with an Agilent 6890 GC system coupled to a mass spectrometer equipped with an Agilent 5973 quadrupole mass analyzer. Chromatographic analysis was conducted with an injector temperature of 280 °C and an HP-5 capillary column (30.0 m × 0.25 mm × 0.32 μm) with a helium (99.999%) flow rate of 2.0 ml·min^{-1} and a 1:10 split ratio. The oven was heated using the

following temperature program: initial temperature of 100 °C increased to 250 °C at a heating rate of 5 °C·min^{-1} and maintained for 10 min. The mass spectrometer was operated in electron ionization mode at 70 eV energy.

Table S1. Progress on hydrodeoxygenation of levulinic acid to γ-valerolactone over heterogeneous bimetallic catalyst in the past decade

Entry	Catalyst	Dosage of catalyst (mol·mol^{-1})	Solvent	Temp. (°C)	P_{H2} (MPa)	LA Con. (%)	GVL Yield (%)	Highest TOF[a] (h^{-1})	Ref.
1	1 wt% $Ru_{0.5}$-$Pd_{0.5}$/TiO_2	LA/Ru=869.8	dioxane	200	4	＞99	99.6	2160	1
2	1 wt% $Au_{0.5}$-$Pd_{0.5}$/TiO_2	LA/Au=1306	dioxane	200	4	90	87.8	360	1
3	6.2 wt% $Ru_{0.9}$-$Ni_{0.1}$/OMC	LA/Ru=6247	H_2O	150	4.5	99	97	2936	2
4	43.1 wt% $Ni_{0.58}$-$Sn_{0.42}$/AlOH	LA/Ni=13.4	H_2O	120	4	＞99	＞99	6.6	3
5	2.5 wt% $Ni_{0.35}$-$Ru_{0.65}$/γ-Al_2O_3	LA/Ru=22.9	solvent-free	150	HCOOH	71	71	10.8	4
6	4 wt% $Pd_{0.65}$-$Au_{0.35}$/Ti-HMS	LA/Pd=343.6	H_2O	160	15	100	99	344	5
7	1 wt% $Au_{0.6}$-$Ru_{0.4}$/AC	LA/Ru=2500	H_2O	70	0.7	87	84	352	6
8	Bulk $Cu_{0.33}$-$Cr_{0.67}$ oxide	LA/Cu=20.3	H_2O	200	7	97.8	90	1.8	7
9	22.14 wt% $Ni_{0.62}$-$Cu_{0.38}$/γ-Al_2O_3	LA/Ni=38.3	H_2O	250	6.5	100	96	18.4	8
10	30 wt% $Pd_{0.02}$-$Cu_{0.98}$/ZrO_2	LA/Pd=31.9	H_2O	200	6	100	70	0.93	9
11	17 wt% $Ni_{0.7}$-$Mo_{0.3}$Ox/AC	LA/Ni=5000	solvent-free	250	5	100	99	206	10
12	6.7 wt% $Ru_{0.57}$-$Re_{0.43}$/AC	LA/Ru=2070	H_2O	160	15	91	85	10557	11
13	20 wt% Ni-Cu/Al_2O_3-ZrO_2	LA/Ni=25.3	2-butanol	220	3	87.4	87.2	66.9	12
14	6 wt% $Fe_{0.34}$-$Re_{0.66}$/TiO_2	LA/Re =24.5	H_2O	180	4	100	95	5.8	13
15	35 wt.% $Ni_{0.66}$-$Cu_{0.34}$/Al_2O_3	LA/Ni =49	Solvent-Free	220	3	100	＞99	8.1	14
16	20 wt% $Cu_{0.7}$-$Co_{0.3}$/Al_2O_3	LA/ Cu =103.2	Solvent-Free	250	0.1	91.3	90.5	23.3	15
17	20 wt%$Ni_{0.75}$-$Fe_{0.25}$/Fe_3O_4	LA/Ni =6.5	isopropanol	130	2	93.8	89.6	2.9	16
18	5wt %$Ni_{0.8}$-$Pd_{0.2}$(Cl)/γ-Al_2O_3	LA/Ni =21.1	H_2O	190	HCOOH	56	51	5.4	17
19	12.1 wt%$Cu_{0.37}$-$Ag_{0.63}$/γ-Al_2O_3	LA/Ag =24.5	tetrahydrofuran	180	1.4	100	＞99	6.1	18
20	20 wt%$Cu_{0.62}$-$Ni_{0.22}$/Mg/Al	LA/Cu =22.1	dioxane	140	3	100	100	7.4	19
21	5 wt%$Au_{0.2}$–$Ni_{0.8(Cl)}$/γ-$Al_2O_{3(C)}$	LA/Ni =42.1	H_2O	190	1	62	60	12.6	20
22	20 wt%$Cu_{0.2}$-$Ni_{0.8}$/SiO_2	LA/Ni =378.1	solvent-free	250	0.1	98.2	95.9	45.2	21
23	33 wt%$Cu_{0.66}$-$Ni_{0.33}$/SiO_2	LA/Cu=5.7	isopropanol	120	4	99.3	96.1	396	22
24	66 wt% $Ni_{0.67}Cu_{0.34}$/Al_2O_3	GHSV=11.34	H_2O	275	0.1	99.9	99.9	19.5[b]	23
25	1.2 wt% $Pd_{0.16}Ru_{0.84}$/TiO_2	LA/Ru=1000	H_2O	65	0.1	93.3	93.3	322	14
26	8 wt% $Ni_{0.61}Fe_{0.39}$/SBA-15	LA/(Ni+Fe)=24.6	Methanol	200	1	100	>99	874	24

27	20 wt% $Ni_{0.15}Co_{0.85}/\gamma\text{-}Al_2O_3$	WHSV=3.42 h^{-1}	solvent-free	250	0.1	78.8	75.8	57.2[c]	[25]
28	1 wt% $Co_{0.5}Re_{0.5}/TiO_2$	LA/Co=1760	dioxane	220	1.5	100	＞99	1328	Our work

[a] TOF was re-calculated based on the yield of GVL and the metal mentioned in the second column in a batch reactor. While in a fixed-bed reactor, TOF was presented without re-calculation.

[b] Re-calculated based on Ni and Cu.

[c] Re-calculated based on Ni and Co.

Table S2. Co 2p and Re 4f dispersion on different catalysts.

Catalyst	Elemental Species	Binding Energy (eV)	Content
Re/TiO_2	ReO $4f_{5/2}$	41.7	74%
	ReO_2 $4f_{5/2}$	42.7	11%
	Re_2O_5 $4f_{5/2}$	43.3	15%
	ReO $4f_{7/2}$	44.1	
	ReO_2 $4f_{7/2}$	45.3	
	Re_2O_5 $4f_{7/2}$	45.9	
Co/TiO_2	Co $2p_{1/2}$	778.2	15%
	CoO $2p_{1/2}$	781	42%
	CoO $2p_{1/2}$ shakeup	786.1	44%
	Co $2p_{3/2}$	793.3	
	CoO $2p_{3/2}$	796.6	
	CoO $2p_{3/2}$ shakeup	802.3	
$Co_{0.5}Re_{0.5}/TiO_2$	ReO $4f_{5/2}$	41.5	70%
	ReO_2 $4f_{5/2}$	42.5	12%
	Re_2O_5 $4f_{5/2}$	43.1	18%
	ReO $4f_{7/2}$	43.9	
	ReO_2 $4f_{7/2}$	45.1	
	Re_2O_5 $4f_{7/2}$	45.7	
	Co $2p_{1/2}$	778.4	16%
	CoO $2p_{1/2}$	781.2	39%
	CoO $2p_{1/2}$ shakeup	786.3	45%
	Co $2p_{3/2}$	793.5	
	CoO $2p_{3/2}$	796.8	
	CoO $2p_{3/2}$ shakeup	802.5	
spent $Co_{0.5}Re_{0.5}/TiO_2$	ReO $4f_{5/2}$	41.5	66%
	ReO_2 $4f_{5/2}$	42.5	12%
	Re_2O_5 $4f_{5/2}$	43.1	22%
	ReO $4f_{7/2}$	43.9	
	ReO_2 $4f_{7/2}$	45.1	
	Re_2O_5 $4f_{7/2}$	45.7	
	Co $2p_{1/2}$	778.4	16%
	CoO $2p_{1/2}$	781.2	40%
	CoO $2p_{1/2}$ shakeup	786.3	44%
	Co $2p_{3/2}$	793.5	
	CoO $2p_{3/2}$	796.8	
	CoO $2p_{3/2}$ shakeup	802.5	

Table S3. H_2-TPD results of $CoRe/TiO_2$ bimetallic catalysts with various Co:Re molar ratios

Catalyst	Weight (g)	Metal loading (wt%)	Content (wt%)		H_2 uptake ($ml \cdot g^{-1}$/STP)	mole of H_2 (10^{-6} $mol \cdot g^{-1}$)	Dispersion based on	
			Co	Re			Co (%)	Re(%)
Co/TiO_2	0.1125	1	1	0	0.0892	3.47	18.2	
$Co_{0.8}Re_{0.2}/TiO_2$	0.1073	1	0.927	0.0733	0.200	7.80	46.2	
$Co_{0.5}Re_{0.5}/TiO_2$	0.1089	1	0.760	0.240	0.303	11.8	84.0	
$Co_{0.2}Re_{0.8}/TiO_2$	0.1070	1	0.441	0.559	0.0906	3.52	43.9	
Re/TiO_2	0.1080	1	0	1	0.0218	0.850		14.6

Note: H_2-TPD of the catalysts was determined by a temperature programmed desorption technology. About 100 mg of catalyst were reduced at 500 °C for 2 h, and then cooled down and swept with hydrogen stream at room temperature for 30 min. After that, the hydrogen in system was replaced by helium, and then heated to 800 ºC by 5 ºC·min^{-1} in a helium flow of 25 ml·min^{-1}. The H_2 desorption species (m/z =2) were detected by an online mass spectrometry.

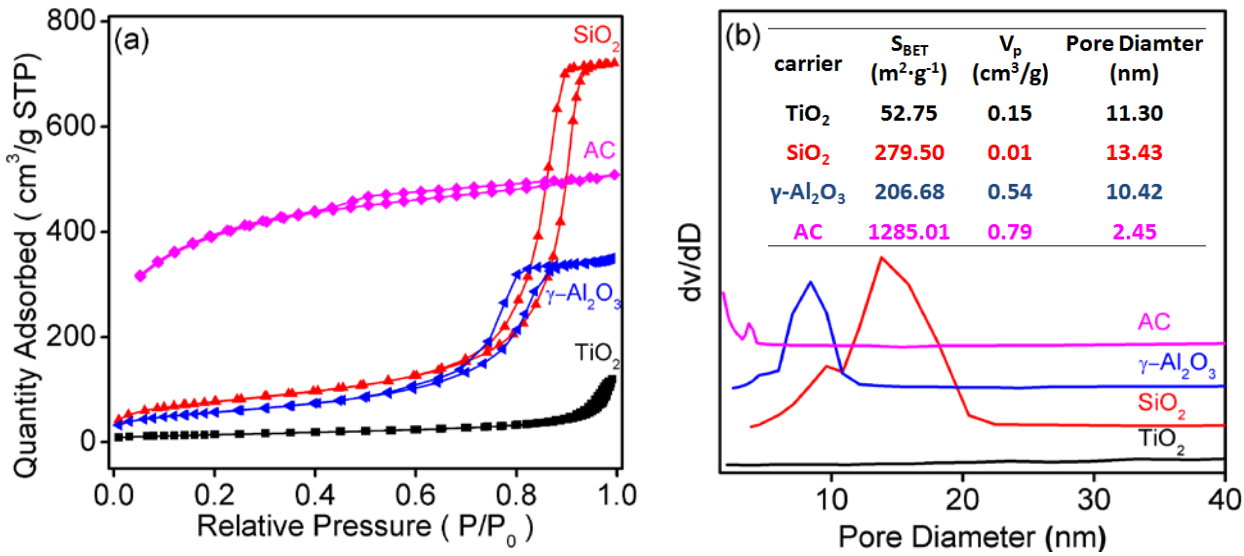

Figure S1. (a) Nitrogen adsorption-desorption isotherms and (b) the BJH pore size distributions of TiO_2, AC, γ-Al_2O_3 and SiO_2.

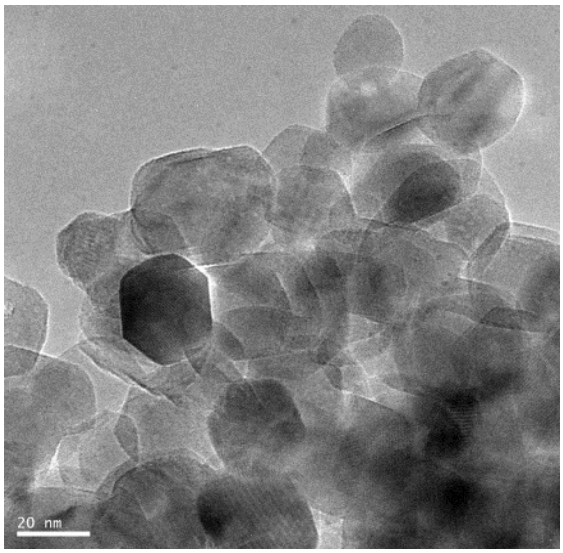

Figure S2. TEM images of 1 w% $Co_{0.5}$-$Re_{0.5}/TiO_2$ catalyst.

For a nonporous TiO_2 sphere with diameter of d=25 nm and true density of D=4 g·cm^{-3}, the specific exterior surface area can be calculated as:

$$\alpha = \frac{\pi d^2}{(\pi d^3/6)\cdot D} = \frac{6}{25\ \mathrm{nm}\cdot 4\ \mathrm{g}\cdot \mathrm{cm}^{-3}} = 60\ \mathrm{m}^2\cdot \mathrm{g}^{-1}$$

Since the BET specific surface area of the TiO_2 was 52.75m^2·g^{-1}, which is quite close to the specific exterior surface area of TiO_2 with similar size, we therefore consider that the nano TiO_2 support we used is nonporous.

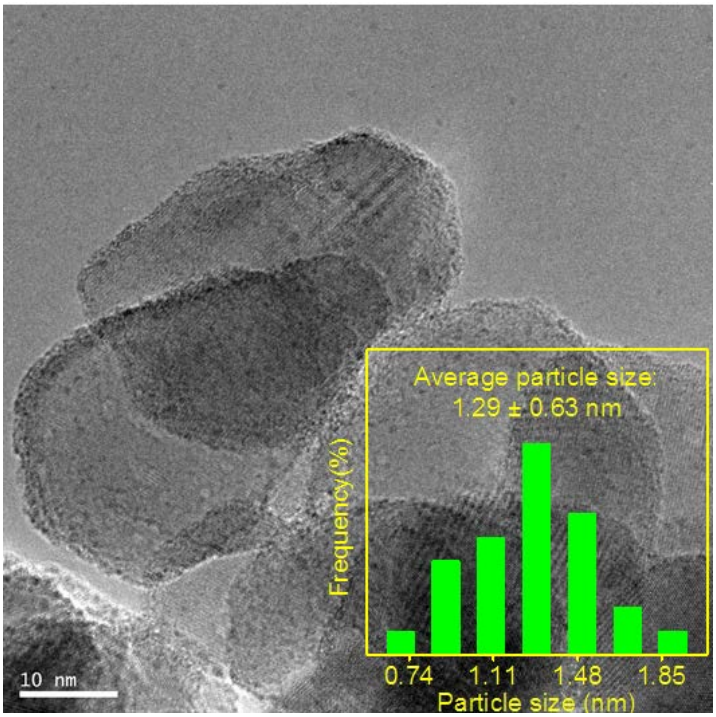

Figure S3. TEM image of four-recycled 1 wt% $Co_{0.5}Re_{0.5}/TiO_2$ catalyst

References

1. Luo, W.; Sankar, M.; Beale, A. M.; He, Q.; Kiely, C. J.; Bruijnincx, P. C.; Weckhuysen, B. M., High performing and stable supported nano-alloys for the catalytic hydrogenation of levulinic acid to gamma-valerolactone. *Nat. Commun.* **2015,** *6*, 7540.

2. Yang, Y.; Gao, G.; Zhang, X.; Li, F., Facile fabrication of composition-tuned Ru–Ni bimetallics in ordered mesoporous carbon for levulinic acid hydrogenation. *ACS Catal.* **2014,** *4* (5), 1419-1425.

3. Rodiansono; Astuti, M. D.; Hara, T.; Ichikuni, N.; Shimazu, S., Efficient hydrogenation of levulinic acid in water using a supported Ni-Sn alloy on aluminium hydroxide catalysts. *Catal. Sci. Technol.* **2016,** *6* (9), 2955-2961.

4. Al-Naji, M.; Yepez, A.; Balu, A. M.; Romero, A. A.; Chen, Z.; Wilde, N.; Li, H.; Shih, K.; Glaeser, R.; Luqueb, R., Insights into the selective hydrogenation of levulinic acid to γ-valerolactone using supported mono- and bimetallic catalysts. *J. Mol. Catal. A: Chem.* **2016,** *417*, 145-152.

5. Testa, M. L.; Corbel-Demailly, L.; La Parola, V.; Venezia, A. M.; Pinel, C., Effect of Au on Pd supported over HMS and Ti doped HMS as catalysts for the hydrogenation of levulinic acid to γ-valerolactone. *Catal. Today* **2015,** *257*, 291-296.

6. Villa, A.; Chan-Thaw, C. E.; Campisi, S.; Bianchi, C. L.; Wang, D.; Kotula, P. G.; Kubel, C.; Prati, L., AuRu/AC as an effective catalyst for hydrogenation reactions. *Phys. Chem. Chem. Phys.* **2015,** *17* (42), 28171-28176.

7. Yan, K.; Chen, A., Efficient hydrogenation of biomass-derived furfural and levulinic acid on the facilely synthesized noble-metal-free Cu–Cr catalyst. *Energy* **2013,** *58*, 357-363.

8. Obregón, I.; Corro, E.; Izquierdo, U.; Requies, J.; Arias, P. L., Levulinic acid hydrogenolysis on Al_2O_3-based Ni-Cu bimetallic catalysts. *Chinese J. Catal.* **2014,** *35* (5), 656-662.

9. Patankar, S. C.; Yadav, G. D., Cascade engineered synthesis of γ-valerolactone, 1,4-pentanediol, and 2-methyltetrahydrofuran from levulinic acid using Pd–Cu/ZrO_2 catalyst in water as solvent. *ACS Sustainable Chemistry & Engineering* **2015,** *3* (11), 2619-2630.

10. IShimizu, K.-i.; Kanno, S.; Kon, K., Hydrogenation of levulinic acid to γ-valerolactone by Ni and MoOxco-loaded carbon catalysts. *Green Chem.* **2014,** *16* (8), 3899-3903.

11. Corbel-Demailly, L.; Ly, B.-K.; Minh, D.-P.; Tapin, B.; Especel, C.; Epron, F.; Cabiac,

A.; Guillon, E.; Besson, M.; Pinel, C., Heterogeneous Catalytic Hydrogenation of Biobased Levulinic and Succinic Acids in Aqueous Solutions. *ChemSusChem* **2013,** *6* (12), 2388-2395.

12. Xie, Z.; Chen, B.; Wu, H.; Liu, M.; Liu, H.; Zhang, J.; Yang, G.; Han, B., Highly efficient hydrogenation of levulinic acid into 2-methyltetrahydrofuran over Ni-Cu/Al_2O_3-ZrO_2 bifunctional catalysts. *Green Chem.* **2019,** *21* (3), 606-613.

13. Huang, X. M.; Liu, K. T.; Vrijburg, W. L.; Ouyang, X. H.; Dugulan, A. I.; Liu, Y. X.; Verhoeven, M.; Kosinov, N. A.; Pidko, E. A.; Hensen, E. J. M., Hydrogenation of levulinic acid to gamma-valerolactone over Fe-Re/TiO_2 catalysts. *Appl. Catal. B: Environ.* **2020,** *278*, 119314.

14. Xu, G. Y.; Li, C.; Deng, T. Y.; Wang, C. G.; Zhang, Y.; Fu, Y., Kinetic Studies on the Impact of Pd Addition to Ru/TiO_2 Catalyst: Levulinic Acid to gamma-Valerolactone under Ambient Hydrogen Pressure. *Ind. Eng. Chem. Res.* **2020,** *59* (39), 17279-17286.

15. Yanase, D.; Yoshida, R.; Kanazawa, S.; Yamada, Y.; Sato, S., Efficient formation of γ-valerolactone in the vapor-phase hydrogenation of levulinic acid over Cu-Co/alumina catalyst. *Catal. Commun.* **2020,** *139*, 105967.

16. Wang, H.; Chen, C.; Zhang, H.; Wang, G.; Zhao, H., An efficient and reusable bimetallic Ni3Fe NPs@C catalyst for selective hydrogenation of biomass-derived levulinic acid to γ-valerolactone. *Chinese J. Catal.* **2018,** *39* (10), 1599-1607.

17. Soszka, E.; Reijneveld, H. M.; Jędrzejczyk, M.; Rzeźnicka, I.; Grams, J.; Ruppert, A. M., Chlorine Influence on Palladium Doped Nickel Catalysts in Levulinic Acid Hydrogenation with Formic Acid as Hydrogen Source. *ACS Sust. Chem. Eng.* **2018,** *6* (11), 14607-14613.

18. Zhang, L.; Mao, J.; Li, S.; Yin, J.; Sun, X.; Guo, X.; Song, C.; Zhou, J., Hydrogenation of levulinic acid into gamma-valerolactone over in situ reduced CuAg bimetallic catalyst: Strategy and mechanism of preventing Cu leaching. *Appl. Catal. B: Environ.* **2018,** *232*, 1-10.

19. Gupta, S. S. R.; Kantam, M. L., Selective hydrogenation of levulinic acid into γ-valerolactone over Cu/Ni hydrotalcite-derived catalyst. *Catal. Today* **2018,** *309*, 189-194.

20. Ruppert, A. M.; Jędrzejczyk, M.; Potrzebowska, N.; Kaźmierczak, K.; Brzezińska, M.; Sneka-Płatek, O.; Sautet, P.; Keller, N.; Michel, C.; Grams, J., Supported gold-nickel nano-alloy as a highly efficient catalyst in levulinic acid hydrogenation with formic acid as an internal hydrogen source. *Catal. Sci. Technolog.* **2018,** *8* (17), 4318-4331.

21. Yoshida, R.; Sun, D.; Yamada, Y.; Sato, S., Stable Cu-Ni/SiO_2 catalysts prepared by using citric acid-assisted impregnation for vapor-phase hydrogenation of levulinic acid. *Mol. Cat.* **2018,** *454*, 70-76.

22. Pendem, S.; Mondal, I.; Shrotri, A.; Rao, B. S.; Lingaiah, N.; Mondal, J., Unraveling the structural properties and reactivity trends of Cu-Ni bimetallic nanoalloy catalysts for biomass-derived levulinic acid hydrogenation. *Sustain. Energy Fuels* **2018,** *2* (7), 1516-1529.

23. Gundeboina, R.; Velisoju, V. K.; Gutta, N.; Medak, S.; Aytam, H. P., Influence of surface Lewis acid sites for the selective hydrogenation of levulinic acid to gamma-valerolactone over Ni-Cu-Al mixed oxide catalyst. *React. Kinet. Mech. Catal.* **2019,** *127* (2), 601-616.

24. Luo, L. G.; Han, X.; Zeng, Q., Hydrogenative Cyclization of Levulinic Acid to gamma-Valerolactone with Methanol and Ni-Fe Bimetallic Catalysts. *Catalysts* **2020,** *10* (9), 1096.

25. Kondeboina, M.; Enumula, S. S.; Reddy, K. S.; Challa, P.; Burri, D. R.; Kamaraju, S. R. R., Bimetallic Ni-Co/gamma-Al_2O_3 catalyst for vapour phase production of gamma-valerolactone: Deactivation studies and feedstock selection. *Fuel* **2021,** *285*, 119094.